Hall and bend resistance of a phosphorene Hall bar

L. P. Miranda,[1,2,*] S. P. Milovanović,[2] R. N. Costa Filho,[1] and F. M. Peeters[2]
[1]*Departamento de Física, Universidade Federal do Ceará, Campus do Pici, 60455-760 Fortaleza, Ceará, Brazil*
[2]*Department of Physics, University of Antwerp, Groenenborgerlaan 171, B-2020 Antwerp, Belgium*

(Received 1 April 2021; revised 31 May 2021; accepted 11 June 2021; published 1 July 2021)

The dependence of the Hall and bend resistances on a perpendicular magnetic field and on vacancy defects in a four-terminal phosphorene single layer Hall bar is investigated. A tight-binding model in combination with the Landauer-Büttiker formalism is used to calculate the energy spectrum, the lead-to-lead transmissions, and the Hall and bend resistances of the system. It is shown that the terminals with zigzag edge orientation are responsible for the absence of quantized plateaus in the Hall resistance and peaks in the longitudinal resistance. A negative bend resistance in the ballistic regime is found due to the presence of high- and low-energy transport modes in the armchair and zigzag terminals, respectively. The system density of states, with single vacancy defects, shows that the presence of in-gap states is proportional to the number of vacancies. Quantized plateaus in the Hall resistance are only formed in a sufficiently clean system. The effects of different kinds of vacancies where the plateaus are destroyed and a diffusive regime appears in the bend resistance are investigated.

DOI: 10.1103/PhysRevB.104.035401

I. INTRODUCTION

In pursuit of the next generation of nanodevices and to continue its downscaling, scientists have started to focus their attention on two-dimensional (2D) materials due to their nanoscale thickness [1]. Among these materials, black phosphorus, which in ambient is the most stable phosphorus crystal at room temperature and pressure, has drawn a lot of attention recently due to its unique electronic properties which depend on the number of layered phosphorene [2,3]. Black phosphorus is a layered material where each individual atomic layer is held together by van der Waals interactions [4–6]. This allows the construction of phosphorene devices with an arbitrary number of layers [6,7]. Each phosphorus atom in a phosphorene monolayer is bounded via sp^3 hybridization forming a puckered lattice structure. Unlike other 2D layered materials, black phosphorus shows interesting properties such as high carrier mobility [3,6], anisotropic optical-conductance [8,9], and a band-gap dependence on the number of layers [9,10], ranging from 0.3 eV for bulk and 1.5 eV for monolayer phosphorene. This material also has a good on/off switch, which makes it a good candidate for field effect transistor (FET) devices [11,12].

The above-mentioned phosphorene FET devices were analyzed at room temperature through Hall measurements with mobility up to $\sim 1000\,\mathrm{cm}^2\,\mathrm{V}^{-1}\,\mathrm{s}^{-1}$. It was found that the carrier mobility is limited by charge impurities at low temperature [12]. It is important to mention that Hall measurements can accurately determine the carrier density, electrical resistivity, and the mobility of carriers in semiconductors [13]. It is well known that 2D electron gas submitted to a perpendicular magnetic field leads to the formation of Landau levels and, as a consequence, it leads to the formation of quantized levels and oscillations in the Hall and longitudinal conductivity/resistance [13–15]. With the application of a perpendicular magnetic field, it is also possible to focus electrons injected from a narrow injector, allowing the study of different properties of a material [16] in such a magnetic focusing experiment.

The presence of defects is almost inevitable in materials. In particular, vacancies in phosphorene were reported to exhibit a highly anisotropic and delocalized charge density, with intrinsic vacancies resulting in in-gap resonance states [17–19]. In the absence of a magnetic field, the effects of different types of vacancies in phosphorene monolayers were theoretically investigated in multiterminal systems, showing that the presence of atomic defects decrease (an increase) the longitudinal (transverse) conductance [20,21]. Studies on graphene showed that vacancy disorder can cause the appearance of new states in the Landau spectrum, which depend on the type and density of vacancies, which can be observed in the bend resistance and the density of states (DOS) [22]. To provide insights on how vacancies affect the transport properties of phosphorene, we analyze the different resistances in a Hall bar configuration.

In this paper, the problem of magnetotransport in multiterminal phosphorene monolayer is addressed. This will be done by studying the resistance of a four-terminal Hall bar system in the presence of a perpendicular magnetic field. This paper is organized as follows. First, we present in Sec. II the theoretical formalism to calculate the different resistances in a Hall bar using the Landauer-Büttiker formalism [23] and the tight-binding model to describe the phosphorene lattice [24]. In Sec. III, the results for a pristine Hall bar with an applied perpendicular magnetic field is presented. In Sec. IV the effect of vacancies on the DOS and the transport properties are

*lucasmiranda@fisica.ufc.br

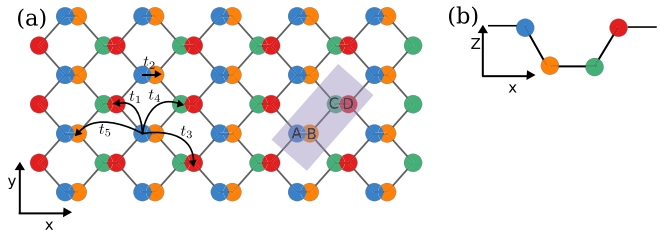

FIG. 1. The phosphorene nanoribbon along the *xy* plane (a), and the representation in the *zx* plane (b). The different hoppings are shown in (a) and the rectangular shaded box gives the unit cell. The colored dots refer to *P* atoms belonging to different sublattices.

investigated. The perspectives and conclusions are presented in Sec. V.

II. SYSTEM AND METHODS

A. Phosphorene

The unit cell of phosphorene contains four atoms, with $a_1 = 3.32$ Å and $a_2 = 4.38$ Å being the primitive vectors and $a = 2.22$ Å and $\theta = 96.79^{\circ}$ are the in-plane bond length and bond angle, see Fig. 1. For our numerical simulations, we use the tight-binding model with five-hoppings as introduced in Ref. [24]. The tight-binding Hamiltonian is given by

$$H = \sum_i \epsilon_i n_i + \sum_{i \neq j} t_{ij} c_i^{\dagger} c_j, \tag{1}$$

where the sums run over the lattices sites, $c_i^{\dagger}(c_j)$ is the creation (annihilation) operator, ϵ_i is the electron on-site energy, and t_{ij} are the elements of the hopping matrix. Because all phosphorene atoms are equivalent, we may set the on-site energy to zero. The five hopping parameters are given by $t_1 = -1.220$ eV, $t_2 = 3.665$ eV, $t_3 = -0.205$ eV, $t_4 = -0.105$ eV, and $t_5 = -0.055$ eV. They describe the band structure of phosphorene in the low-energy regime and agree with the one obtained from DFT-GW calculations [24].

The peculiar electronic properties of the phosphorene band structure is shown in Fig. 2(a) for the armchair edge and Fig. 2(b) for the zigzag edge, both with width $W = 50$ nm. The main difference between the two orientations is the presence of a quasiflat band within the band gap in the nanoribbon with zigzag edges resulting in metallic behavior [25,26], while the band structure for the armchair terminal is semiconducting. The corresponding DOS are also shown.

The phosphorene monolayer is modeled using a four-band tight-binding model, but can be reduced to a two-band model due to the symmetry between the sublattices *A* and *D* [27] [see Fig. 1]. In this reduced form, the number of atoms in sublattices, labeled *A* and *B* for convenience, are N_A and N_B. For pristine phosphorene monolayer (without defects), $N_A = N_B$ (sublattice symmetry). In this system, vacancies are introduced by randomly removing atoms from the phosphorene lattice, eliminating the on-site energy and the hopping of the removed atom. Figure 3 shows sections of the defective phosphorene Hall bar with three types of atomic vacancies: A monovacancy (MV) where a single sublattice atom is removed, a type-I double vacancy (DV1) where an atom and its

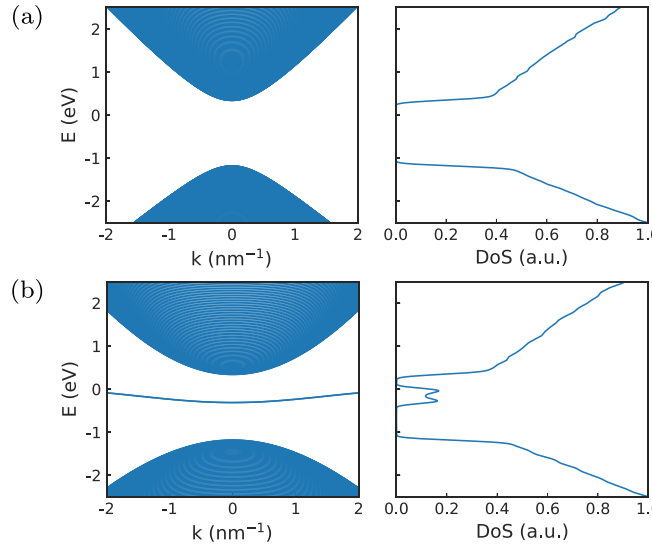

FIG. 2. Phosphorene nanoribbon band structure and density of states for armchair (a) and zigzag (b) edges. The nanoribbons correspond to the different leads in the investigated Hall bar with width 50 nm.

neighbor sublattice atom on a different *z* plane are removed, and a type-II double vacancy (DV2) where the neighbor sublattice atom is removed on the same *z* plane.

In the MV case, where only one of the sublattice atoms is removed, the sublattice symmetry is broken ($N_A \neq N_B$). For the type-I DV, where two sublattice atoms are removed, being two *A* (or two *B*), the sublattice symmetry is also broken ($N_A \neq N_B$). However for type II, where one *A* and one *B* are removed, the symmetry is preserved ($N_A = N_B$).

B. Hall bar

The Hall device is schematically presented in Fig. 4. It is a four-terminal Hall bar system with an applied magnetic field in the *z* direction, where the magnetic field is introduced through the vector potential.

The Landau gauge $\vec{A}_H = -By\vec{e}_x$ is one of the standard gauges which works only for leads with translational symmetry in *x* direction. For *y*-translational symmetry, we need to change it to the gauge $\vec{A}_V = Bx\vec{e}_y$. The change from one gauge to the other is done smoothly by implementing the scalar function $f(x, y)$ which rotates the vector potential $\vec{A}' = \vec{A} + \vec{\partial} f$, where *f* is defined as [22,28]

$$f(x, y) = Bxy \sin^2\theta + \tfrac{1}{4}B(x^2 - y^2)\sin 2\theta. \tag{2}$$

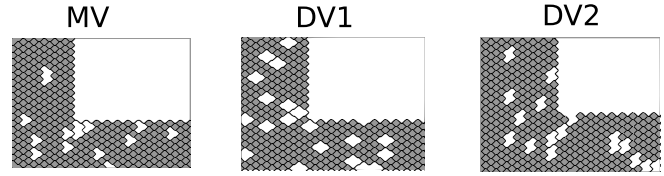

FIG. 3. The disorders in phosphorene Hall bar for monovacancies (MVs), double vacancy type I (DV1) and type II (DV2). Only half of the Hall bar is shown.

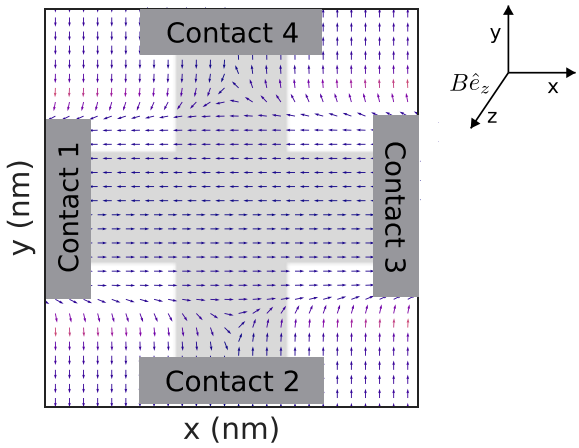

FIG. 4. Schematic representation of the Hall bar. The modified vector field $\vec{A}'(x, y)$ is shown by the arrows. In the system, contacts 1 and 3 represent the armchair terminals while contacts 2 and 4 the zigzag terminals.

Here θ is the angle between the two leads (in our system $\theta = \pi/2$). To apply $f(x, y)$ only in the main region, we multiply it by a smooth step function $\epsilon_i(y) = \frac{1}{2}[1 + \tanh(2(y - y_0)/d)]$, which is nonzero only close to the lead i. y_0 is the crossover position and d is the width of the crossover region. For our numerical calculations, we took $y_0 = W$ and $d = W/5$, where $W = 50$ nm [22]. The modified magnetic field is then implemented on the tight-binding Hamiltonian Eq. (1) by making use of the Peierls substitution $t_{ij} = t_{ij}e^{i\phi_{ij}}$. The Peierls phase is then described as

$$\phi_{ij} = \int_{\vec{r}_j}^{\vec{r}_i} \vec{A} \cdot d\vec{r}. \tag{3}$$

The resistances are calculated using Landauer-Büttiker formula [29]. The four-terminal resistance in a cross-shaped structure is given by

$$R_{mn,kl} = \frac{h}{2e^2}\left(\frac{T_{km}T_{ln} - T_{kn}T_{lm}}{D}\right), \tag{4}$$

where h is the Planck's constant. $R_{mn,kl}$ is the resistance with the voltage being measured between the leads k and l when the current is driven into contact m and taken out from contact n. In Eq. (4), $D = (\alpha_{11}\alpha_{22} - \alpha_{12}\alpha_{21})S$, with

$$\alpha_{11} = [(T_{21} + T_{31} + T_{41})S - (T_{14} + T_{12})(T_{41} + T_{21})]/S,$$
$$\alpha_{12} = (T_{12}T_{34} - T_{14}T_{32})/S,$$
$$\alpha_{21} = (T_{21}T_{43} - T_{41}T_{23})/S,$$
$$\alpha_{22} = [(T_{12} + T_{32} + T_{42})S - (T_{21} + T_{23})(T_{32} + T_{12})]/S,$$

where $S = T_{12} + T_{14} + T_{32} + T_{34}$, and T_{ij} is the transmission probability from lead j to lead i. The resistances given by Eq. (4) satisfy the relation $R_{mn,lk} = R_{nm,kl}$ and the reciprocity relation $R_{mn,kl}(B) = R_{kl,mn}(-B)$ [29]. In this paper, we are also going to analyze the longitudinal resistance defined as $R_{13,13}$ ($R_{24,24}$), which represents the resistance between the two opposite armchair (zigzag) terminals. This schematic can also be calculated, in a first approximation [30], by the analogous two-terminal systems, where the resistance is simply proportional to the transmission between the terminals [13,30].

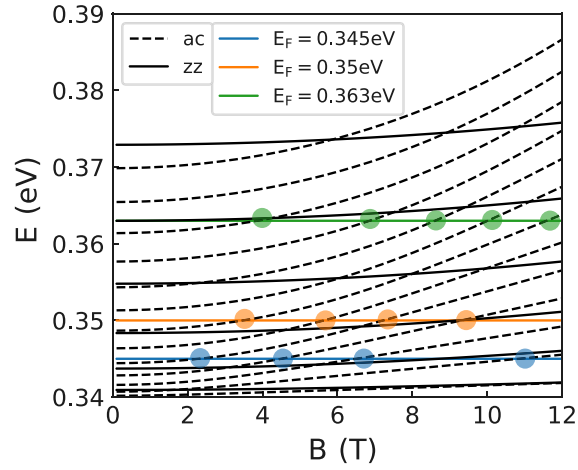

FIG. 5. The phosphorene energy levels for nanoribbons as function of magnetic field. The nanoribbons with width $W_{ac} = 50$ nm and $W_{zz} = 50$ nm correspond to the semi-infinite leads in the Hall bar. The points in the figure indicate the intersection of the Fermi energy (E_F) with the Landau levels.

The probabilities T_{ij} are numerically calculated using KWANT [31], a software package for numerical calculation of tight-binding systems with emphasis on quantum transport. It uses a matching wave-function approach [32] to calculate the transmission of an n-propagating mode in a contact terminal to the m mode in another contact. This formulation is mathematically equivalent to the nonequilibrium Green's function but was found to be numerically more stable [31].

III. PRISTINE PHOSPHORENE HALL BAR

Due to the anisotropy of the lattice, the Landau-level splitting depends strongly on the orientation and the edge type of the phosphorene nanoribbon [8,26]. This dependency is

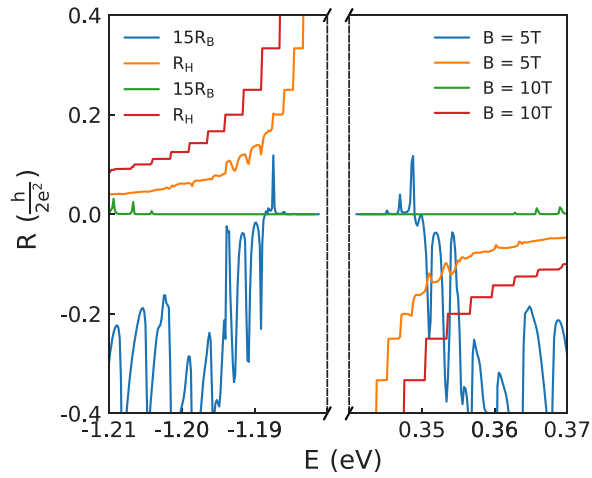

FIG. 6. Hall ($R_{13,42}$) and bend ($R_{14,23}$) resistance dependency on the Fermi energy for two different values of the magnetic field.

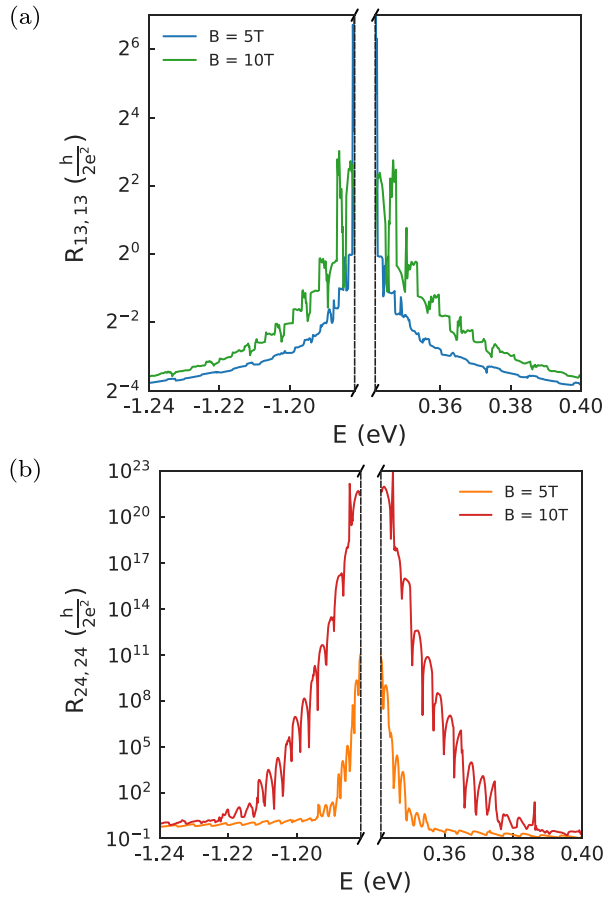

FIG. 7. Longitudinal resistance, measured for the armchair terminals ($R_{13,13}$) and for the zigzag terminals ($R_{24,24}$), varying with the Fermi energy for two different values of the magnetic field.

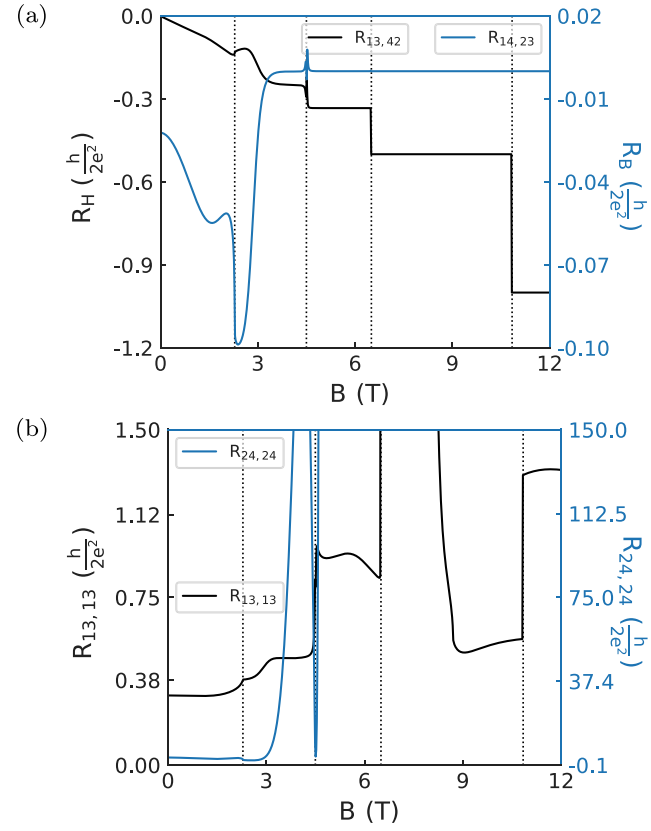

FIG. 8. (a) Hall (black), bend (blue), and (b) longitudinal (blue) resistances for a pristine phosphorene Hall bar for $E_F = 0.345$ eV. The vertical dashed lines mark the points where the Fermi energy crosses the armchair Landau levels.

shown in Fig. 5, where the electron energy spectrum for the armchair (ac) and zigzag (zz) nanoribon is plotted against the magnetic field for nanoribbons with width $W = 50$ nm. For the zigzag orientation, the effective electron mass is much smaller than the one for the armchair nanoribbon. That is the origin of the different spacing and magnetic field dependency of the Landau levels [8,26].

Next, we analyze the resistances for Fermi energy near the intersecting points depicted in Fig. 5. The Hall ($R_{13,42}$) and bend ($R_{14,23}$) resistances were calculated for a Hall bar with terminals size 50 nm (with a total of 342 384 atoms in the system). Figure 6 shows the resistance dependence on the Fermi energy ($E_F > 0$ for electrons and $E_F < 0$ for holes) for two different values of the applied magnetic field (5 T and 10 T). As the energy approaches the edges of the band, one can see the Hall resistance goes to infinity while the bend resistance goes to zero. The transition between the two plateaus in the Hall resistance indicate the points where the Fermi energy crosses a semiconductor transverse mode (see Fig. 5) formed due the presence of magnetic field. Notice that at such points the bend resistance exhibits a negative dip. Another interesting phenomena is the presence of negative values in the bend resistance, indicating a ballistic regime (the ballistic regime will be discussed further when analyzing the resistances as a function of magnetic field).

To study the effect of the ribbon orientation, the longitudinal resistances $R_{13,13}$ and $R_{24,24}$ are shown in Fig. 7. These resistances were calculated using the two-terminal relation for the resistances, which is just the inverse of the transmission between the two opposite terminals. Due to the anisotropic spectrum in phosphorene, one would expect that $\sigma_{xx} < \sigma_{yy}$, leading to $R_{13,13} > R_{24,24}$, but for Hall bar, the opposite happens. This is due to the presence of a scattering region in the Hall bar that affects the conductivity making $\sigma_{xx} > \sigma_{yy}$ and also $R_{13,13} < R_{24,24}$, as explained in Ref. [21] for a cross-shaped phosphorene nanoribbon.

Next, we investigate the different resistances as a function of the magnetic field for a fixed Fermi energy. It is well known that as the magnetic field increases, the Fermi energy crosses the semiconductor (armchair) transverse modes, resulting in well-defined plateaus in the Hall resistance [8]. In the system studied here, this behavior is clear for $E_F = 0.345$ eV and 0.34 eV (Figs. 8 and 9). However, for $E_F = 0.363$ eV (Fig. 10), the plateaus in the Hall resistance are almost absent for a weak magnetic field. This can be explained by looking at Fig. 5. The Fermi energy $E_F = 0.363$ (eV) is near to a zigzag transverse mode, which is almost magnetic-field independent [8]. Due to the metallic character, zigzag terminals induce scattering between the transport modes, not allowing the formation of quantized plateaus in the Hall resistance [21]. However, as the magnetic field increases, the energy of the

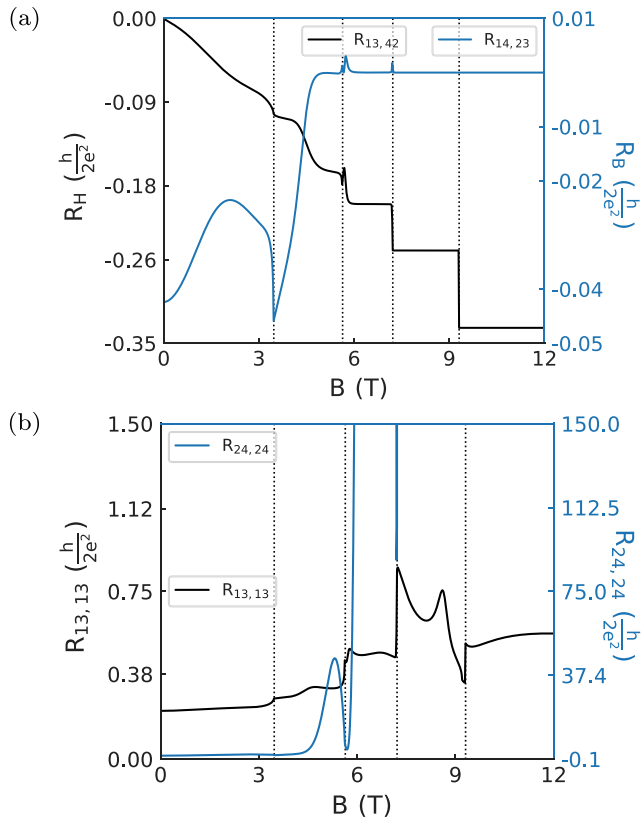

FIG. 9. (a) Hall (black) and bend (blue) and (b) Hall (black) and longitudinal (blue) resistances for the pristine phosphorene Hall bar for $E_F = 0.35$ eV. The vertical dashed lines marks the points where the Fermi energy crosses the armchair Landau levels.

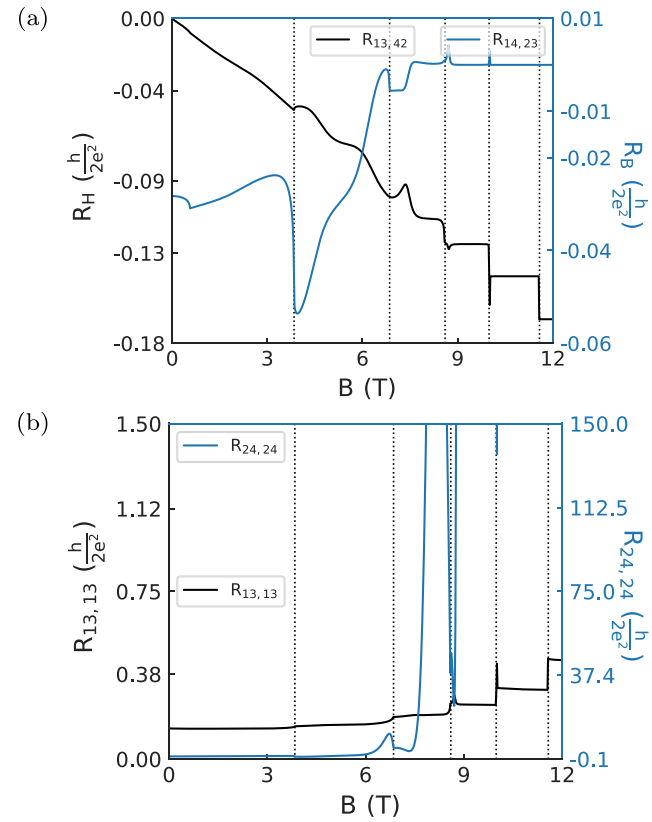

FIG. 10. (a) Hall (black), bend (blue), and (b) Hall (black) and longitudinal (blue) resistances for the pristine phosphorene Hall for $E_F = 0.363$ eV. The vertical dashed lines mark the points where the Fermi energy crosses the armchair Landau levels.

zigzag Landau level differs from the Fermi energy, and the plateaus on the Hall bar are recovered.

The ballistic regime observed in Fig. 6 becomes more evident when analyzing the magnetic-field dependency reported in Figs. 8–10. The bend resistances are plotted in panel (a) (blue curve) which goes to zero as the magnetic field increases. A negative bend resistance indicates that the electron trajectory does not bend to the closer nonaxial terminal [33,34]. We can understand this negative value by considering the definition of the four-terminal resistance as $R_{ij,km} = V_{km}/I_{ij}$ [29]. For $R_{14,23}$, we have $V_{23} = V_2 - V_3$, indicating that $V_{23} < 0$, as V_2 is a zigzag (lower energy) terminal and V_3 is an armchair (high energy) terminal. Even though the bend resistance approaches zero, one can still see peaks in the resistances, indicating an increase in the transmission between axial terminals. These peaks happens whenever the Fermi energy cross an armchair transverse mode, indicating an increase in the *xx* conductivity.

As stated before, the $R_{24,24}$ is larger than $R_{13,13}$, and they increase with different rates as the magnetic field increases. Figures 8–10 also show that for strong magnetic fields, the bend resistances go to zero while $R_{24,24}$ takes larger values. Another peculiar behavior for $R_{13,13}$ is noticed when the Fermi energies 0.345 eV and 0.35 eV cross the zigzag transverse mode (respectively, at ∼8.0 T and ∼8.60 T). When that happens, a peak appears in $R_{13,13}$.

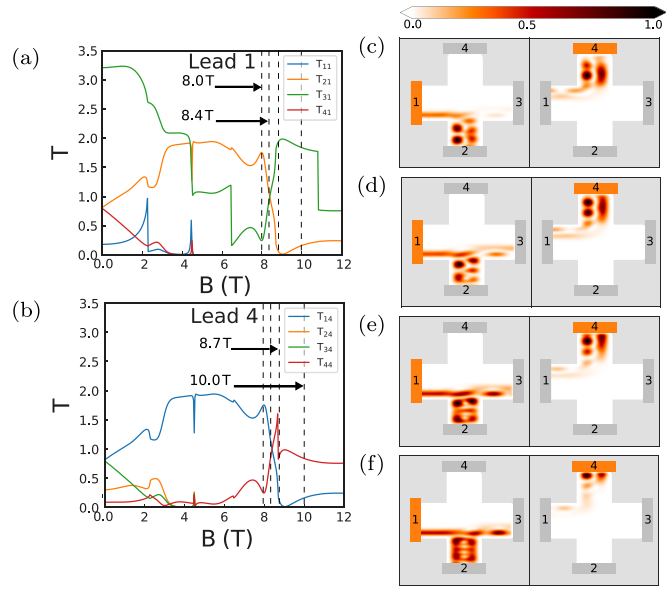

FIG. 11. The transmission probability from the leads 1 (a) and 4 (b) to the other leads. The local current density is calculated for specific magnetic fields 8.0, 8.4, 8.7, and 10.0 T, respectively, (c)–(f). Density values were normalize, as shown by the in the color bar. The Fermi energy is $E_F = 0.345$ eV.

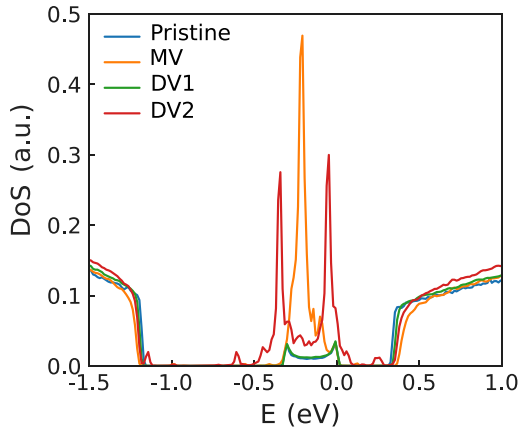

FIG. 12. DOS of the phosphorene Hall bar for pristine and for three types of disorder with $n_x = 1\%$.

To understand the appearance of these peaks, Fig. 11 shows the magnetic-field dependency of the different transmissions probabilities between the leads for $E_F = 0.345$ eV. An expected behavior is the decrease of T_{ij} between two counterclockwise terminals as the magnetic field increases. The transmission between the two armchair terminals suddenly increases as the transmission with the next counterclockwise zigzag transmission decreases. This behavior is an indication of the induced transport-mode scattering by the zigzag terminals. Also, the reflection probability of the zigzag transport modes increase with magnetic field.

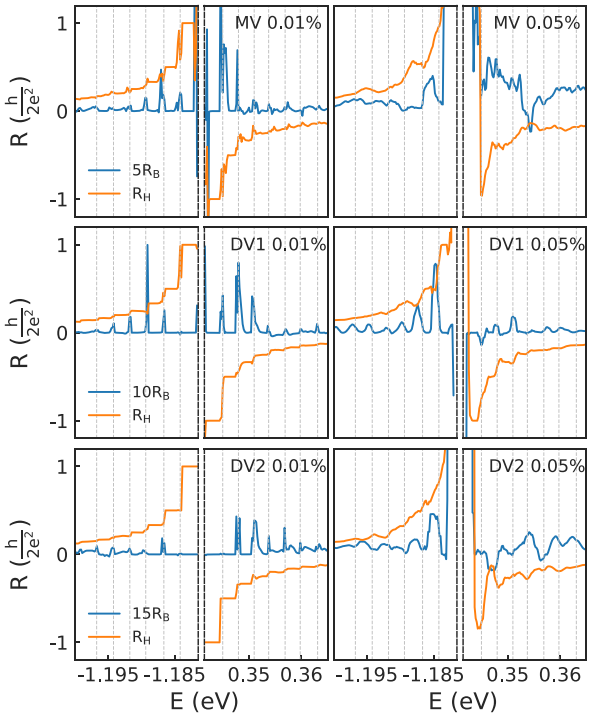

FIG. 13. Hall and bend resistances for the phosphorene Hall bar with different densities of vacancies for $B = 10$ T. The bend resistances were multiplied by a defined factor to increase its visibility. The grey vertical lines mark the place where the Fermi energy crosses an armchair transverse mode.

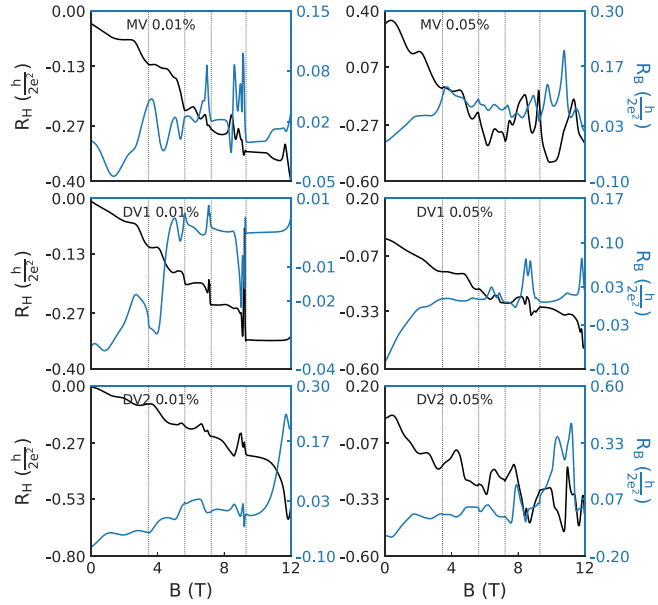

FIG. 14. The magnetic-field dependency of the Hall and bend resistances for the phosphorene Hall bar with vacancies at fixed Fermi energy $E_F = 0.35$ eV.

IV. EFFECT OF VACANCIES

Figure 12 shows the DOS for a phosphorene Hall bar with MVs and DVs type I and II (see Sec. II). To get reasonable statistics, the DOS was averaged over ten samples where the vacancies are randomly distributed. The number of vacancies

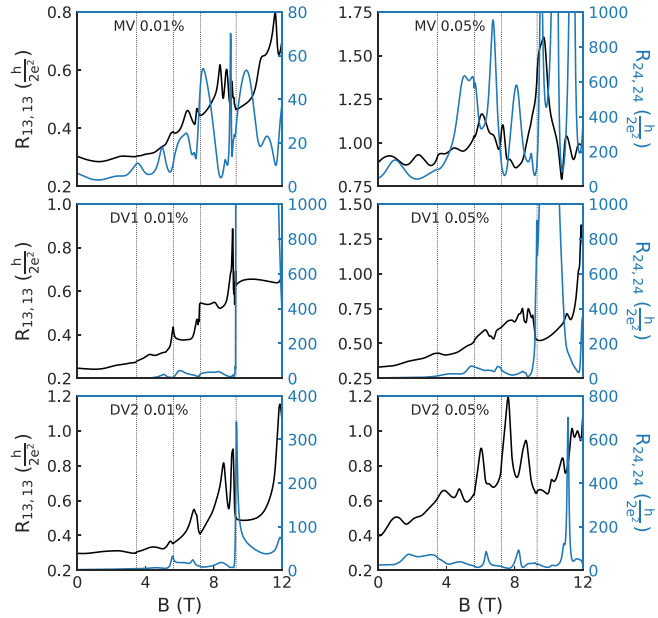

FIG. 15. The magnetic-field dependency of the longitudinal resistance for the phosphorene Hall bar with vacancies at fixed Fermi energy $E_F = 0.35$ eV.

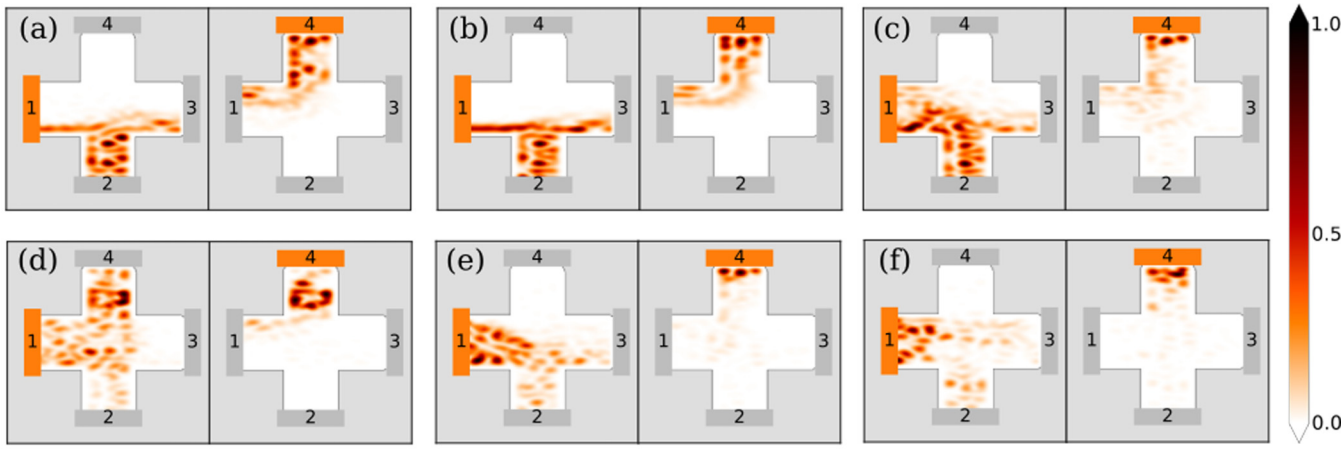

FIG. 16. Current density for the phosphorene Hall bar with vacancy defects MV (a), DV1 (b), and DV2 (c) for $n_x = 0.01\%$ and MV (d), DV1 (e), and DV2 (f) for $n_x = 0.05\%$. We fixed $E_F = 0.35$ eV and $B = 10$ T.

is related to the quantity n_x, which is defined as the ratio between the atoms removed from the lattice and the total number of atoms. The peaks shown in Fig. 12 for the MV and DV2 systems are due to in-gap states. The intensity of the DOS is proportional to the number of defects [18,35].

Although there are no transport modes inside the gap, the in-gap defect states can affect the system's conductivity via vacancy scattering [20,36]. This is shown in Fig. 13, where the Hall and bend resistances are plotted against the Fermi energy for two different values of vacancy density with an applied magnetic field $B = 10$ T. Each resistance was obtained as an average $R = \sum_i^N R_i/N$, for $N = 10$ random samples. For $n_x = 0.01\%$, we can still see the presence of plateaus in the Hall resistance, but it vanishes for $n_x = 0.05\%$ due to scattering.

Another interesting result is the presence of well-defined peaks in the bend resistance, peaks that were not present in the pristine case (see Fig. 8). This indicates that already for small vacancy density, the system is in the diffusive regime. These peaks, unlike in the case in graphene [22], are not due to localization states. They occur when the Fermi energy cross an armchair transverse mode and are related to the increase of diffusion due to the vacancy scattering. Also, this effect is more evident for MV disorder, as for the same vacancy density the MV are more spread in the system than DV1 and DV2.

The DV1 does not create in-gap defect states and the resistances change slightly when compared with the pristine case. This behavior becomes more evident in Fig. 14. The Landau plateaus are more resilient in DV1 and the range of the bend resistance is of the same order of magnitude as in the pristine case, while for MV and DV2 the bend resistances are higher. Further, one can see that the presence of the defects with broken symmetry actually suppress the scattering effect provoked by the zigzag transport modes. Analyzing Fig. 15, one notices that the increase in the longitudinal resistance $R_{24,24}$ at ~9.3 T is smaller for MV and DV2, and also with the increase of density in DV1. Thus, one can infer that the presence of resonant states reduces the scattering provoked by the zigzag terminals. Apart from these specific effects, the general behavior is that the MV and DV2 enhances the resistances between two axial terminals. This behavior is in agreement with Ref. [21]. To better understand this effect, we show in Fig. 16 the local density of the transport modes for a system with MV, DV1, and DV2 defects for $n_x = 0.01\%$ and 0.05% and magnetic field $B = 10$ T. As the density is increased, the modes are scattered to nonaxial terminals, which is reflected by the enhancement of the longitudinal resistance.

V. CONCLUSIONS

In summary, we analyzed the electrical transport properties of a phosphorene Hall bar in the presence of a magnetic field and vacancy defects. The presence of axial and nonaxial terminals, with different characteristics, allowed us to study different transport properties of phosphorene material [21,37] (in this case, the Hall and longitudinal resistances). In Sec. III, we studied the pristine system where a ballistic regime was identified by the bend resistance to certain regimes of Fermi energy and magnetic field, and Landau plateaus show up in the Hall resistance mainly due the semiconductor features of the armchair terminals [8,21]. This can be seen for magnetoresistance for $E_F = 0.363$ eV which matches a zigzag transport mode (see Fig. 5) and shows no Landau plateaus for the Hall resistance (see Fig. 10). Also, as stated in Ref. [21], the presence of zigzag transport modes provokes scattering of the transport modes, resulting in a larger peak in the resistance as the Fermi energy crosses the zigzag Landau level, see Fig. 11.

The presence of vacancies changes the magnetotransport properties, depending on the sublattice symmetry and on the vacancy density, as shown in Sec. IV. The effects on the resistance are most noticeable for vacancy types with broken sublattice symmetry, with the MV being the one that most affects the resistance. Although DV1 does not create in-gap states (as shown in Fig. 12) the defects still affect the phosphorene transport properties. When analyzing the magnetoresistance, a change in the sign of the bend resistance appears, which indicates a diffusive regime induced by scattering from the defects. The present paper clearly indicates the much richer transport features that can be observed in phosphorene as compared to graphene. The anisotropy of the phosphorene lattice and the presence of a gap are responsible for the increased complexity of its electrical response.

ACKNOWLEDGMENTS

The authors are grateful to the National Counsel of Scientific and Technological Development (CNPq) and to the National Council for the Improvement of Higher Education (CAPES) of Brazil for financial support. L.P.M is supported by CAPES/PRINT, Finance Code No. 364590/2019-00. R.N.C.F is supported by CNPq Grant No. 312384/2018-1. Part of this work was supported by the Flemish Science Foundation (FWO-Vl).

[1] D. Akinwande, C. Huyghebaert, C.-H. Wang, M. Serna, S. Goossens, L. Li, H.-S. Wong, and F. Koppens, Nature **573**, 507 (2019).

[2] A. Castellanos-Gomez, L. Vicarelli, E. Prada, J. Island, K. Narasimha-Acharya, S. Blanter, D. Groenendijk, M. Buscema, G. Steele, J. Alvarez, H. Zandbergen, J. Palacios, and H. Zant, 2D Mater. **1**, 025001 (2014).

[3] J. Qiao, X. Kong, Z.-X. Hu, F. Yang, and W. Ji, Nat. Commun. **5**, 4475 (2014).

[4] A. Carvalho, M. Wang, X. Zhu, A. Rodin, H. Su, and A. Castro Neto, Nat. Rev. Mater. **1**, 16061 (2016).

[5] P. Chen, N. Li, X. Chen, W.-J. Ong, and X. Zhao, 2D Mater. **5**, 014002 (2017).

[6] M. Akhtar, G. Anderson, R. Zhao, A. Alruqi, J. Mroczkowska, G. Sumanasekera, and J. Jasinski, npj 2D Mater. Appl. **1**, 5 (2017).

[7] S. Dhanabalan, J. Ponraj, Z. Guo, S. Li, and Q. Bao, Adv. Sci. **4**, 1600305 (2017).

[8] X. Y. Zhou, R. Zhang, J. P. Sun, Y. L. Zou, D. Zhang, W. K. Lou, F. Cheng, G. H. Zhou, F. Zhai, and K. Chang, Sci. Rep. **5**, 12295 (2015).

[9] D. Çakır, C. Sevik, and F. M. Peeters, Phys. Rev. B **92**, 165406 (2015).

[10] H. Liu, A. Neal, Z. Zhu, Z. Luo, X. Xu, D. Tomanek, and P. Ye, ACS Nano **8**, 4033 (2014).

[11] L. Li, Y. Yu, G. Ye, Q. Ge, O. Xuedong, H. Wu, D. Feng, X. Chen, and Y. Zhang, Nat. Nanotechnol. **9**, 372 (2014).

[12] L. Li, G. J. Ye, V. Tran, R. Fei, G. Chen, H. Wang, J. Wang, K. Watanabe, T. Taniguchi, L. Yang, X. H. Chen, and Y. Zhang, Nat. Nanotechnol. **10**, 608 (2015).

[13] S. Datta, *Electronic Transport in Mesoscopic Systems*, Cambridge Studies in Semiconductor Physics and Microelectronic Engineering (Cambridge University Press, Cambridge, UK, 1995).

[14] J. M. Pereira, Jr. and M. I. Katsnelson, Phys. Rev. B **92**, 075437 (2015).

[15] M. Tahir, P. Vasilopoulos, and F. M. Peeters, Phys. Rev. B **92**, 045420 (2015).

[16] S. Milovanovic, M. Ramezani Masir, and F. Peeters, J. Appl. Phys. **115**, 043719 (2014).

[17] B. Kiraly, N. Hauptmann, A. Rudenko, M. Katsnelson, and A. Khajetoorians, Nano Lett. **17**, 3607 (2017).

[18] Y. Liu, F. Xu, Z. Zhang, E. S. Penev, and B. I. Yakobson, Nano Lett. **14**, 6782 (2014).

[19] Y. Liu, T. Low, and P. P. Ruden, Phys. Rev. B **93**, 165402 (2016).

[20] L. L. Li and F. M. Peeters, Phys. Rev. B **97**, 075414 (2018).

[21] N. A. Shah, L. L. Li, V. Mosallanejad, F. M. Peeters, and G.-P. Guo, Nanotechnology **30**, 455705 (2019).

[22] M. D. Petrović and F. M. Peeters, Phys. Rev. B **94**, 235413 (2016).

[23] Y. Imry and R. Landauer, Rev. Mod. Phys. **71**, S306 (1999).

[24] A. Rudenko and M. Katsnelson, Phys. Rev. B **89**, 201408(R) (2014).

[25] A. Carvalho, A. S. Rodin, and A. H. C. Neto, Europhys. Lett. **108**, 47005 (2014).

[26] M. Ezawa, J. Phys.: Conf. Ser. **603**, 012006 (2015).

[27] D. J. P. de Sousa, L. V. de Castro, D. R. da Costa, J. M. Pereira, and T. Low, Phys. Rev. B **96**, 155427 (2017).

[28] O. Shevtsov, P. Carmier, C. Petitjean, C. Groth, D. Carpentier, and X. Waintal, Phys. Rev. X **2**, 031004 (2012).

[29] M. Büttiker, Phys. Rev. Lett. **57**, 1761 (1986).

[30] D. K. Ferry, S. M. Goodnick, and J. Bird, *Transport in Nanostructures*, 2nd ed. (Cambridge University Press, Cambridge, UK, 2009).

[31] C. W. Groth, M. Wimmer, A. R. Akhmerov, and X. Waintal, New J. Phys. **16**, 063065 (2014).

[32] M. Zwierzycki, P. Khomyakov, A. Starikov, K. Xia, M. Talanana, P. Xu, V. Karpan, I. Marushchenko, I. Turek, E. Bauer, G. Brocks, and P. Kelly, Phys. Status Solidi B **245**, 623 (2008).

[33] Y. Takagaki, F. Wakaya, S. Takaoka, K. Gamo, K. Murase, and S. Namba, Jpn. J. Appl. Phys. **28**, 2188 (1989).

[34] S. Weingart, C. Bock, U. Kunze, F. Speck, T. Seyller, and L. Ley, Appl. Phys. Lett. **95**, 262101 (2009).

[35] S. Yuan, A. N. Rudenko, and M. I. Katsnelson, Phys. Rev. B **91**, 115436 (2015).

[36] M. Amini, M. Soltani, E. Ghanbari-Adivi, and M. Sharbafiun, Europhys. Lett. **125**, 67001 (2019).

[37] B. Ostahie and A. Aldea, Phys. Rev. B **93**, 075408 (2016).